Olli Holmgren, Tapani Makkonen, Jouni V. Knuuttila, Mikko Kalo, Victor P. Plessky, and William Steichen. 2007. Side radiation of Rayleigh waves from synchronous SAW resonators. IEEE Transactions on Ultrasonics, Ferroelectrics, and Frequency Control, volume 54, number 4, pages 861-869.

Side Radiation of Rayleigh Waves from Synchronous SAW Resonators

Olli Holmgren, *Student Member, IEEE*, Tapani Makkonen, *Member, IEEE*, Jouni V. Knuuttila, Mikko Kalo, Victor P. Plessky, *Senior Member, IEEE*, and William Steichen

***Abstract*—Surface acoustic wave (SAW) resonators on lithium tantalate ($LiTaO_3$) and lithium niobate ($LiNbO_3$) are investigated. The amplitude of the acoustic fields in the resonators are measured using a scanning laser interferometer. The amplitude profiles of the surface vibrations reveal the presence of distinct acoustic beams radiated from the transducer region of the SAW resonators and propagating with low attenuation. We suggest that this radiation is generated by the charges accumulating at the tips of the finger electrodes. The periodic system of sources, namely oscillating charges at the fingertips, generates Rayleigh-wave beams in the perpendicular and oblique directions. Green's function theory is used to calculate the coupling strength and slowness of the Rayleigh waves on 42°Y-cut $LiTaO_3$ and Y-cut $LiNbO_3$ substrates as a function of the propagation direction. Furthermore, the propagation angles of the Rayleigh-wave beams as a function of frequency are calculated. The computed angles are compared with the measured ones for both the $LiTaO_3$ and $LiNbO_3$ substrates.**

I. Introduction

Surface acoustic wave (SAW) devices operating at radio frequencies are widely used in modern mobile communication systems. In particular, resonators using leaky SAW (LSAW) on lithium tantalate ($LiTaO_3$) and lithium niobate ($LiNbO_3$) may be used to construct resonator filters, such as ladder-type filters. In the ladder SAW filters, the performance of the resonators at frequencies close to the resonance and the antiresonance determines the insertion loss of the device. Therefore, identifying different loss mechanisms and minimizing the losses within the resonator is important in order to improve the performance of ladder-type SAW filters.

Loss mechanisms in SAW resonators may be divided into two categories: electric and acoustic losses. The dominating electric loss mechanism is the resistance of the narrow finger electrodes in the interdigital transducer (IDT). The acoustic losses include viscous losses in the substrate and in the metal electrodes. Possible additional acoustic loss mechanisms may be found by measuring acoustic fields within the SAW resonator as well as in the vicinity of the resonator. Optical probing is a powerful tool for the task as it provides direct physical information of the acoustic fields within SAW resonators, not obtainable through measuring the electrical response. Furthermore, the vibrations can be studied directly without perturbing the operation of the SAW device.

Recently, acoustic loss mechanisms in synchronous one-port LSAW resonators have been under active study. It is shown that the propagation loss of the LSAW on $LiTaO_3$ may be controlled by varying the electrode thickness and the crystal cut [1]. The influence of bulk-wave radiation on IDT admittance on 42°YX-$LiTaO_3$ has been studied in [2]. Direct measurements of bulk acoustic wave (BAW) radiation in LSAW resonators on $LiTaO_3$ is reported in [3], [4]. One critical loss mechanism in LSAW resonators on rotated Y-cut $LiTaO_3$ is the leakage of LSAW into busbar first published in [5], [6]. This phenomenon was later experimentally verified by Wakana *et al.* [7] and Shiba *et al.* [8]. Different acoustic loss mechanisms in LSAW resonators on $LiTaO_3$ are thoroughly discussed in [9], including LSAW leakage into busbars, coupling to BAWs, and Rayleigh-wave radiation. However, the Rayleigh-wave radiation is only briefly discussed from the theoretical point of view. Rayleigh-wave radiation by a thin-film waveguide in the case of Love-wave propagation is treated in [10], but no experimental results are provided.

In this paper, we investigate the acoustic loss mechanism due to the Rayleigh-wave radiation from SAW resonators. The Rayleigh-wave beams are well visible in the acoustic field profiles measured using a laser interferometer [11]. One of the beams is radiated in the direction perpendicular to the resonator (i.e., parallel to the transducer fingers). Others are directed obliquely and symmetrically with respect to the first beam. Using three-dimensional (3-D) Green's function theory, we compute the angular dependence of the velocity and the strength of excitation for Rayleigh waves on 42°Y-cut $LiTaO_3$ and Y-cut $LiNbO_3$ substrates. Furthermore, we calculate the angles of Rayleigh-wave beams emitted from synchronous one-port SAW resonators on these two substrates as a function of frequency. The measured emission angles are compared with calculations.

II. Theory

The theoretical method used in this work is presented in detail in [12]. In the formulation, Biryukov's approach [10]

Manuscript received July 28, 2005; accepted October 27, 2006. This work has been carried out within the Eureka project E! 2442 SUMO: "New Surface Acoustic Wave Filter Generation for Mobile Telecommunications".

O. Holmgren, T. Makkonen, J. V. Knuuttila, and M. Kalo are with Helsinki University of Technology, Espoo, Finland (e-mail: olli.holmgren@tkk.fi).

V. P. Plessky is with GVR Trade SA, Bevaix, Switzerland and with Helsinki University of Technology, Espoo, Finland.

W. Steichen is with Temex, Sophia Antipolis, France.

Digital Object Identifier 10.1109/TUFFC.2007.320

has been adopted, but reformulated in terms of Green's functions [13]. The dyadic Green's function method applied allows one to obtain the complete solution for the electric and elastic fields on the surface and inside the semi-infinite piezoelectric crystal for an arbitrary direction of the surface normal and propagation direction on the surface.

Three-dimensional dyadic Green's functions for SAW device analysis has been actively studied recently by many researchers. A Green's function analysis for SAW devices and the existence theorems of SAWs on piezoelectric substrates has been published by Peach [14], [15]. Green's functions for SAW device analysis also has been studied in [16], for multilayer SAW substrates in [17], and for a laminar plate in [18]. Green's functions theory also has been formulated using compliance/stiffness matrix method [19] and reflection matrix method [20]. The computation of the harmonic spatial-domain Green's function at the surface of a piezoelectric half-space is published in [21] to provide tools for 3-D finite element method/boundary element method (FEM/BEM) algorithms.

A. Eigenproblem Formulation

Consider a semi-infinite homogenous piezoelectric medium occupying the lower half space $z < 0$ such that the surface normal is directed along the positive z-axis. The field variables are assumed to have $e^{i\omega(t-s_x x-s_y y)}e^{-i\omega s_z z}$ dependence, where the components of the surface slowness, s_x and s_y are taken as two independent parameters.

As shown in [14], [17], a wave propagation problem may be expressed as an eigenvalue equation. We have formulated the eigenvalue problem with the unknown z-slowness, s_z, appearing as the eigenvalue:

$$\left[\frac{1}{i\omega}\begin{pmatrix} S_{IJ}^T & -Q_{IJ} \\ K_{IJ} & S_{IJ}\end{pmatrix} - s_z\right]\begin{pmatrix} u_i \\ \phi \\ T_{iz} \\ D_z\end{pmatrix} = 0, \tag{1}$$

where superscript T denotes the transpose of a matrix and u_i, ϕ, T_{iz} and D_z are the components of mechanical displacement, the electric potential, the components of the elastic stress tensor on a plane perpendicular to the z axis, and the z component of electric displacement, respectively. Indices I and J run from 1 to 4. The matrices S_{IJ}, K_{IJ}, Q_{IJ}, containing the material parameters, have the following components:

$$\begin{aligned}
S_{ij} &= -ig_\alpha\left(D_{ij\alpha} + \frac{\tilde{e}_{zi\alpha}\kappa_{jz}}{\tilde{\epsilon}_{zz}}\right),\\
S_{i4} &= +ig_\alpha\frac{\tilde{e}_{zi\alpha}}{\tilde{\epsilon}_{zz}},\\
S_{4j} &= -ig_\alpha\left(\kappa_{j\alpha} - \kappa_{jz}\frac{\tilde{\epsilon}_{\alpha z}}{\tilde{\epsilon}_{zz}}\right),\\
S_{44} &= -ig_\alpha\frac{\tilde{\epsilon}_{\alpha z}}{\tilde{\epsilon}_{zz}},\\
K_{ij} &= +\rho\omega^2\delta_{ij} - g_\alpha g_\beta\left(C_{i\alpha j\beta} - C_{i\alpha zk}D_{jk\beta} + \frac{\tilde{e}_{zj\beta}\tilde{e}_{zi\alpha}}{\tilde{\epsilon}_{zz}}\right),
\end{aligned} \tag{2a}$$

$$\begin{aligned}
K_{i4} &= -g_\alpha g_\beta\left(\tilde{e}_{\beta i\alpha} - \tilde{e}_{zi\alpha}\frac{\tilde{e}_{\beta z}}{\tilde{\epsilon}_{zz}}\right),\\
K_{4j} &= -g_\alpha g_\beta\left(\tilde{e}_{\alpha j\beta} - \tilde{e}_{zj\beta}\frac{\tilde{\epsilon}_{\alpha z}}{\tilde{\epsilon}_{zz}}\right),\\
K_{44} &= +g_\alpha g_\beta\left(\tilde{\epsilon}_{\alpha\beta} - \frac{\tilde{\epsilon}_{\alpha z}\tilde{\epsilon}_{z\beta}}{\tilde{\epsilon}_{zz}}\right),\\
Q_{ij} &= +B_{ij} - \frac{\kappa_{iz}\kappa_{jz}}{\tilde{\epsilon}_{zz}},\ Q_{i4} = +\frac{\kappa_{iz}}{\tilde{\epsilon}_{zz}},\\
Q_{4j} &= +\frac{\kappa_{jz}}{\tilde{\epsilon}_{zz}},\ Q_{44} = -\frac{1}{\tilde{\epsilon}_{zz}},
\end{aligned} \tag{2b}$$

here δ_{ij} is the Kronecker delta symbol and $\mathbf{g} = [g_1\ g_2] = \omega[s_x\ s_y]$ is the surface wave vector. The indices i, j, k, and l run from 1 to 3 and the indices α and β from 1 to 2. The following definitions have been used above:

$$\begin{aligned}
\tilde{\epsilon}_{ij} &= \epsilon_{ij} + e_{ikz}\kappa_{kj} = \tilde{\epsilon}_{ji},\\
\tilde{e}_{ijk} &= e_{ijk} - e_{ilz}D_{jlk} = \tilde{e}_{ikj},\\
\kappa_{ij} &= B_{ik}e_{jkz},\\
D_{ijk} &= C_{ikzl}B_{lj} = D_{kji},\\
B_{ij} &= (C_{izzj})^{-1} = B_{ji},
\end{aligned} \tag{3}$$

where C_{ijkl}, e_{ijk}, and ϵ_{ij} are the components of stiffness, piezoelectric, and permittivity tensors, respectively.

In general, the numerical solution of (1) yields eight different eigenmodes; the modes with a real-valued eigenvalue are bulk-wave modes, and those with a complex-valued eigenvalue are surface-wave modes. The eigenvalues, $s_z^{(n)}(s_x, s_y)$, $n = 1, 2, \ldots, 8$, describe the z-dependence of the field variables, and the corresponding eigenvectors yield the generalized displacements $\mathbf{V}^{(n)}$ and generalized forces $\mathbf{T}^{(n)}$ on the surface of the semi-infinite substrate. From the eight modes, four physical modes in the half space are selected, i.e., bulk modes that feature energy flow into the substrate and surface waves which decay into the substrate. An arbitrary field that is propagating in the substrate with a specific surface slowness, $[s_x\ s_y]$, may be expressed as a linear combination of the four physical eigenmodes.

The dyadic Green's function is constructed from the physical solutions of the eigenproblem (1) [17]:

$$\mathbf{G}^D(s_x, s_y) = \mathbf{V}(s_x, s_y)\mathbf{T}^D(s_x, s_y)^{-1}, \tag{4}$$

where:

$$\begin{aligned}
\mathbf{V} &= \left[\mathbf{V}^{(1)}\ \mathbf{V}^{(2)}\ \mathbf{V}^{(3)}\ \mathbf{V}^{(4)}\right],\\
\mathbf{T}^D &= \left[\mathbf{T}^{(1)}\ \mathbf{T}^{(2)}\ \mathbf{T}^{(3)}\ \mathbf{T}^{(4)}\right],
\end{aligned} \tag{5}$$

are 4×4 matrices with the four eigenvectors as columns. With a change of variables of the generalized force from (T_{iz}, D_z) to (T_{iz}, σ), the fields in upper half space ($z > 0$, assumed to be vacuum) can be included because the surface charge, σ, implicitly contains the responses of both half spaces [15], [22]. The Green's function, $\mathbf{G}^\sigma$, relating

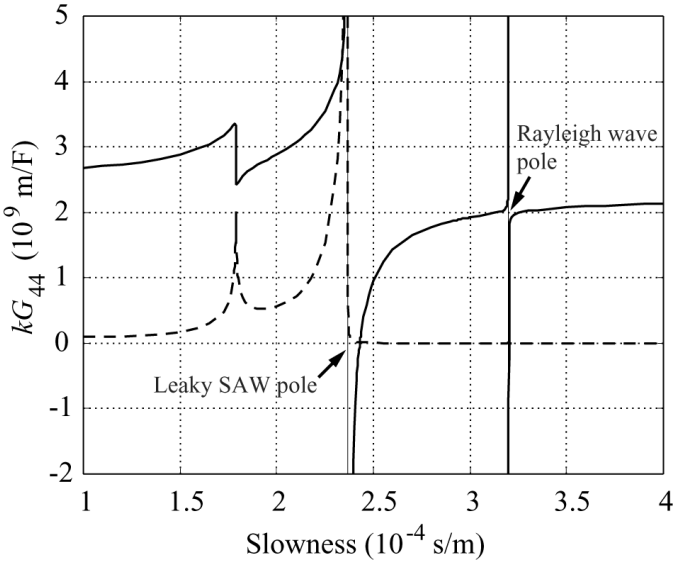

Fig. 1. Scaled component G_{44} for 42°YX-$LiTaO_3$ [Euler angles: (0°, −48°, 0°)]. The propagation direction of the wave is along the positive X axis of the crystal. Solid and dashed curves are the real and imaginary parts, respectively.

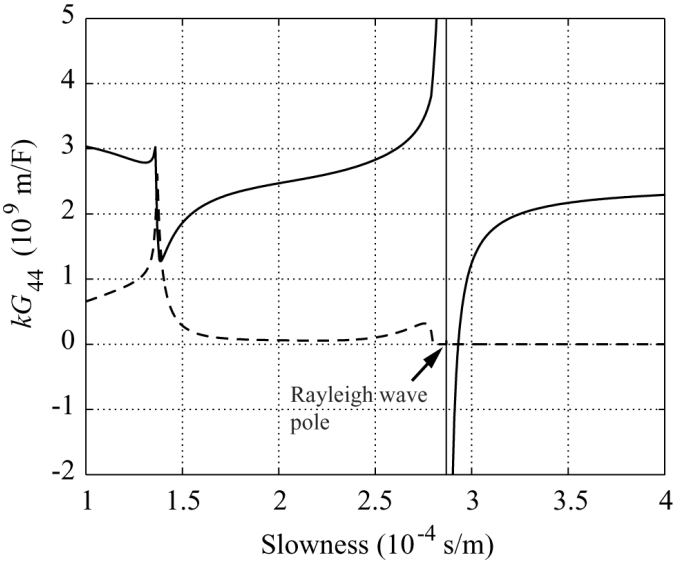

Fig. 2. Scaled component G_{44} for YZ-$LiNbO_3$ [Euler angles: (0°, −90°, −90°)]. The propagation direction of the wave is along the positive Z axis of the crystal. Solid and dashed curves are the real and imaginary parts, respectively.

the generalized displacement, (u_i, ϕ), and the new generalized force, (T_{iz}, σ), can be decomposed into submatrices:

$$\mathbf{G}^{\sigma}(s_x, s_y) = \begin{bmatrix} \mathbf{G}^{\sigma}_{\mathbf{uT}}(s_x, s_y) & \mathbf{G}^{\sigma}_{\mathbf{u}\sigma}(s_x, s_y) \\ \mathbf{G}^{\sigma}_{\phi\mathbf{T}}(s_x, s_y) & G^{\sigma}_{\phi\sigma}(s_x, s_y) \end{bmatrix}, \tag{6}$$

with the mechanical 3×3 part $\mathbf{G}^{\sigma}_{\mathbf{uT}}(s_x, s_y)$, an electric component $G^{\sigma}_{\phi\sigma}(s_x, s_y)$, and the 3×1 and 1×3 piezoelectric parts $\mathbf{G}^{\sigma}_{\mathbf{u}\sigma}(s_x, s_y)$ and $\mathbf{G}^{\sigma}_{\phi\mathbf{T}}(s_x, s_y)$, respectively. The solutions for SAWs on free and metalized surfaces, respectively, are obtained as the poles and zeroes of scaled electric component $G^{\sigma}_{\phi\sigma}(s_x, s_y)/\omega$, referred hereafter to as $G_{44}(s_x, s_y)$.

B. Slowness and Excitation Strength of Rayleigh Waves

The numerically computed scaled electrical component kG_{44} ($k = \omega s$ is the surface wavenumber) of the Green's function is presented as a function of the surface slowness, s, of the wave in Fig. 1 for 42°YX-$LiTaO_3$. Here, the wave propagation is along the crystallographic X axis. The curve shows poles for a piezoelectric Rayleigh wave and for a LSAW, i.e., the substrate supports both the Rayleigh wave and LSAW modes. Fig. 2 shows kG_{44} for YZ-$LiNbO_3$ (wave propagation is along the crystallographic Z axis and surface normal along the crystallographic Y axis). The substrate supports only a piezoelectric Rayleigh wave. A longitudinal leaky SAW (LLSAW) also can be excited on shorted surface, but it features an intrinsic attenuation on the order of 1 dB/wavelength [23]. However, the propagation loss of the LLSAW becomes much lower when a periodic aluminum grating structure with a proper thickness is present on the substrate surface [24]. The high-phase velocity of the LLSAW enables fabrication of 5 GHz SAW ladder filters operating in the fundamental mode using optical lithography [25], [26]. The peaks on the left in Figs. 1 and 2 occuring for slowness values of approximately $1.8 \cdot 10^{-4}$ s/m and $1.4 \cdot 10^{-4}$ s/m, respectively, are due to the threshold for excitation of the longitudinal bulk wave.

The electrical component of the Green's function, ωG_{44}, can be calculated for different propagation directions. From the calculated curves, the poles (s_R) and zeros (s_m) of the ωG_{44} component corresponding to the Rayleigh wave are sought as a function of propagation angle, which yields the slowness curves for free and shorted surfaces, respectively.

In the vicinity of the Rayleigh-wave pole at s_R, it can be assumed that the ωG_{44} component of the Green's function depends on slowness, s, and on propagation angle, θ, as follows [22]:

$$\omega G_{44}(s, \theta) \approx \Gamma(\theta) \left(\frac{1}{s - s_R(\theta)} - \frac{1}{s + s_R(\theta)} \right). \tag{7}$$

From (7), the excitation strength Γ may be estimated as:

$$\frac{1}{\Gamma} \approx s_R \left[\frac{d}{ds} \frac{1}{\omega s G_{44}} \right] \Bigg|_{s = s_R}. \tag{8}$$

The excitation strength Γ is proportional to the coupling parameter $\Delta v/v$ [27]:

$$\Gamma \approx \frac{1}{\epsilon_0 + \epsilon_p^T} \frac{\Delta v}{v}, \tag{9}$$

where ϵ_0 is the permittivity of the free space and ϵ_p^T is defined by $\epsilon_0 = \left(\epsilon_{11}\epsilon_{33} - \epsilon_{13}^2\right)^{1/2}$ with permittivity elements ϵ_{ij} measured at constant stress. The coupling parameter is defined by:

$$\frac{\Delta v}{v} = \frac{v_0 - v_m}{v_0}, \tag{10}$$

where v_0 and v_m are the wave velocities on free surface and on metalized surface, respectively.

C. Radiation Angle of Rayleigh Waves

The angle of the wave vector of the obliquely radiated nth order Rayleigh-wave beams can be approximated on the basis of the synchronism condition between the wavenumber of the grating and that of the Rayleigh waves. The synchronism condition can be expressed in the form:

$$nq_G = \frac{n\pi}{p} = k_x = \omega s_x, \tag{11}$$

where q_G is the wavenumber of the grating, p is the pitch of the transducer, ω is the angular frequency, and k_x and s_x are the x components of the wave vector and slowness of the Rayleigh wave, respectively. Here, the x axis is parallel with the longitudinal direction of the resonator. From (11) we obtain:

$$s_x = \frac{n}{2pf}, \tag{12}$$

where frequency $f = \omega/2\pi$. All the values on the right-hand side of (12) are known. Consequently, from the computed slowness curves we can readily approximate the direction of the wave vector and the slowness vector for the Rayleigh-wave beams. The power flow angle of the Rayleigh-wave beams can be computed as the angle between the outside normal of the slowness curve and the longitudinal direction of the transducer.

III. Measurements

The measurements were carried out using the scanning laser interferometer described in detail in [28]. The interferometer detects the component of mechanical vibrations perpendicular to the surface (vertical component). In addition to the relative vibration amplitude, the mean intensity of the beam reflected from the sample surface is recorded at each scan point. The obtained light-intensity values are used to create a microscope-like image of the scan area (hereafter called light-reflection image).

Two cases are investigated: a LSAW resonator that is part of a 1.9 GHz ladder filter on 42°YX-$LiTaO_3$ and a 1.5 GHz LLSAW test resonator on YZ-$LiNbO_3$. The geometrical parameters of the resonators are summarized in Table I.

Large area scans from the LSAW ladder filter were scanned at 11 different frequencies covering the frequency range from 1740 MHz to 1960 MHz. The measured SAW amplitude profile in a part of the LSAW ladder filter at the frequency of 1781 MHz is shown in Fig. 3. In the image, four oblique beams of Rayleigh waves can be seen clearly, leaving the resonator structure symmetrically with an angle $\alpha \approx 30°$ with respect to the direction parallel to the length of the resonator. Because the probe measures the vertical component of the vibrations, the strength of the

TABLE I
Geometrical Parameters for the Studied Resonators.[1]

Parameter	Resonator	
	LSAW	LLSAW
Substrate	42°YX-$LiTaO_3$	YZ-$LiNbO_3$
Pitch, p (μm)	1.034	2.00
Metalization ratio, m/p	0.65	0.60
Electrode thickness, $h/2p$ (%)	9.9	7.9
Acoustic aperture, W (μm)	24	64
No. of electrodes $N_g/N_t/N_g$	20/211/20	37/151/37

[1] N_g and N_t are the numbers of the finger electrodes in the short-circuited reflector grating and interdigital transducer, respectively.

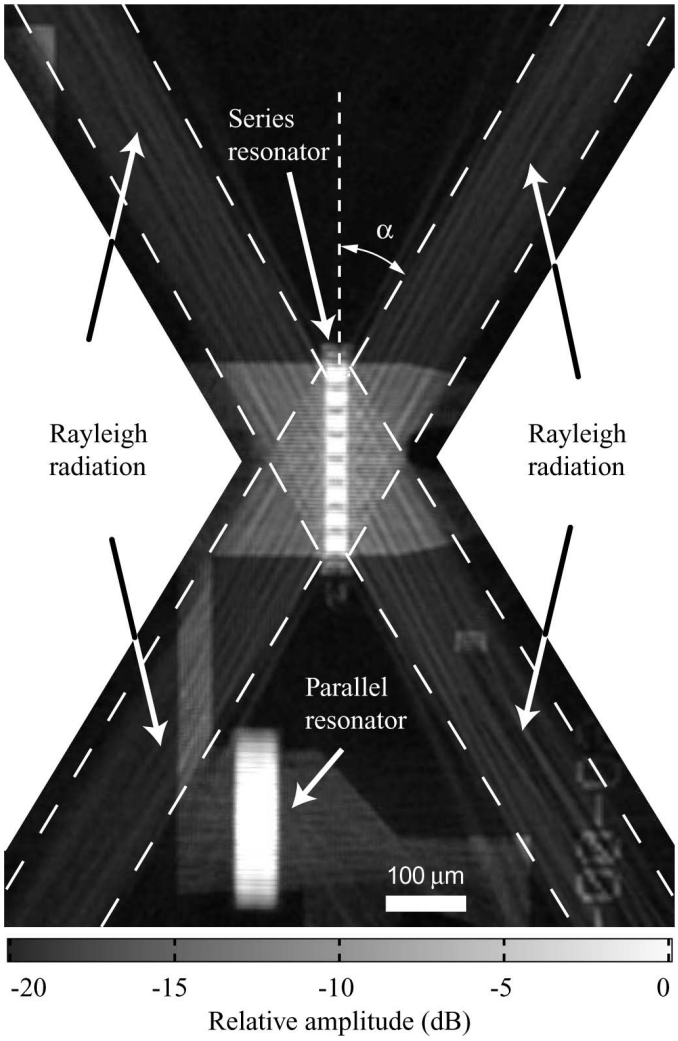

Fig. 3. X-shaped Rayleigh SAW radiation pattern emitted from a series impedance element of a LSAW ladder filter on 42°YX-$LiTaO_3$. The resonator is aligned along the crystallographic X axis (vertical direction in the figure). Note that the sensitivity of the interferometer is different on crystal, on metal, and on grating. Note also the weak Rayleigh-wave beam propagating in the direction perpendicular to the parallel resonator.

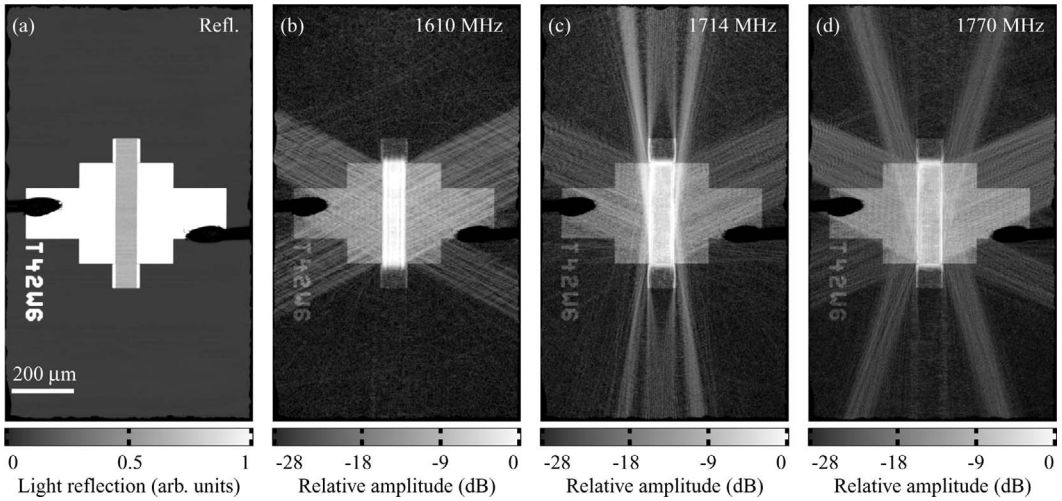

Fig. 4. Selected laser-interferometric scans of the LLSAW resonator on YZ-$LiNbO_3$ (the resonator is aligned along the crystallographic Z axis). (a) Light-reflection image, i.e., light reflectivity of the surface, and relative amplitudes of the vertical vibration component at the frequency (b) 1610 MHz, (c) 1714 MHz, and (d) 1770 MHz. Note that the sensitivity of the interferometer is different on crystal, on metal, and on grating.

Rayleigh wave, for which the vertical component is large, appears pronounced in comparison with the LSAW, for which the dominant displacement component is shear horizontal [29].

It is proposed that the observed beams are generated by the transverse electric fields in the end gaps between the busbars and the electrodes due to oscillating charges accumulated on the electrode fingertips of the IDT. This periodic line of point sources oscillating in phase generates the beams both in the direction perpendicular to the IDT and the first order beams in the oblique directions. The generation of Rayleigh-wave beams through scattering of LSAW at the fingertips or through synchronous coupling of LSAW and Rayleigh waves is unlikely because the Rayleigh-wave radiation from the parallel resonator in Fig. 3 is weak despite the large LSAW amplitude compared to the series resonator. The LSAW amplitude in the parallel resonator is high because the frequency is close to the resonant frequency of the parallel resonator. Practically all the input voltage is applied over the series resonator as the magnitude of the impedance of the parallel resonator is lower than that of the series resonator at this frequency. Due to the higher voltage, the Rayleigh-wave beams emitted from the series resonator are stronger than the ones emitted from the parallel resonator.

For the second sample, the complete chip containing the LLSAW test resonator was scanned at two different frequency ranges. The first set of 48 scanned frequencies covers the frequency range from 790 MHz to 884 MHz, and the second set of 53 scanned frequencies covers the frequency range from 1490 MHz to 1870 MHz. The interesting feature in this sample is that the YZ-$LiNbO_3$ substrate supports two wavemodes. Therefore, in addition to the LLSAW, Rayleigh waves also are excited within the same resonator structure designed for LLSAW operation, but at different frequencies. The resonance frequencies of these two wavemodes are different from each other due to the different wave velocities: 3300 m/s for the Rayleigh wave and 6100 m/s for the LLSAW. For the LLSAW, the resonance frequency is 1540 MHz, and for Rayleigh waves it is 822.9 MHz. For more details, see [30].

The amplitudes of the vertical component of the mechanical vibrations at three selected frequencies are shown in Figs. 4(b), (c), and (d). In the light reflection image in Fig. 4(a), the metalized areas are seen in white and the crystal area in dark gray. The IDT and the reflectors are in the middle of the image. The two black objects in the left and right are the bond wires used to connect the RF voltage to the resonator. At the frequency of 1610 MHz in Fig. 4(b), four oblique beams of Rayleigh waves are clearly seen, emitted from the edges of the resonator to the angle of 64° with respect to the direction of the wave propagation in the resonator (longitudinal direction). At higher frequencies in Figs. 4(c) and (d), four more oblique beams appear. These beams are the second order Rayleigh-wave beams. For example, at 1770 MHz the beams are radiated to the angles of 18° and 67°. The additional beams at the angle of approximately 0° with respect to the longitudinal direction in Fig. 4(c) are due to a part of the second order Rayleigh-wave beams being waveguided by the reflector busbars.

IV. Results

The slowness of the Rayleigh SAW computed as a function of propagation angle θ for the 42°Y-cut $LiTaO_3$ [Euler angles: (0°, −48°, θ)] and for the Y-cut $LiNbO_3$ [Euler angles: (0°, −90°, θ)] are presented in Figs. 5 and 6, respectively. Both cases show nearly isotropic behavior with only a relatively weak dependence on the propagation direction.

The excitation strength of the Rayleigh waves as a function of the propagation angle, calculated from (8), are shown in Figs. 7 and 8 for the 42°Y-cut $LiTaO_3$ and Y-cut

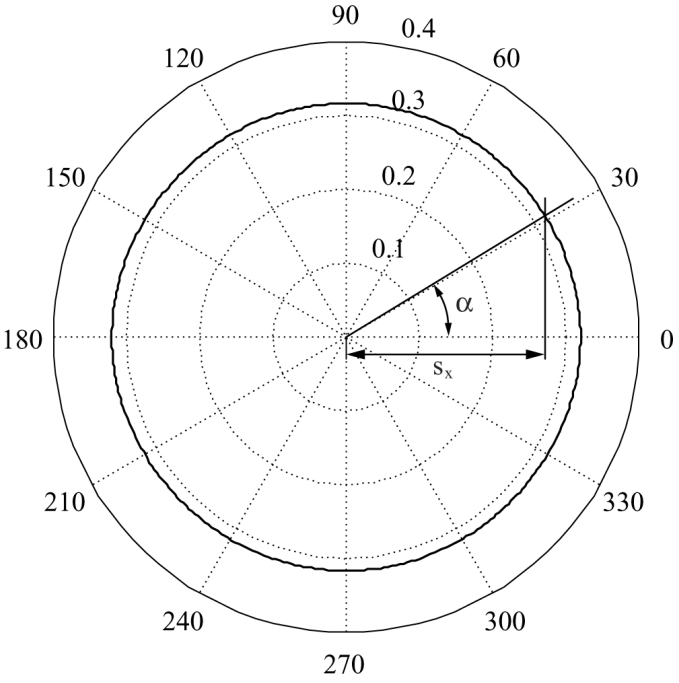

Fig. 5. Rayleigh SAW slowness (in 10^{-3} s/m) for 42°Y-cut $LiTaO_3$ as a function of the propagation direction θ on the shorted substrate surface. s_x is the x component of the surface slowness, and it is parallel with the crystallographic X axis.

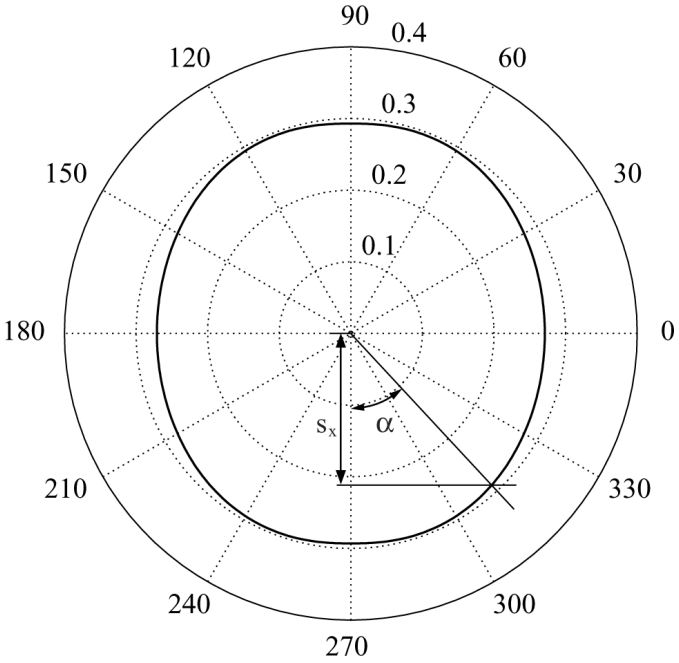

Fig. 6. Rayleigh SAW slowness (in 10^{-3} s/m) for Y-cut $LiNbO_3$ as a function of the propagation direction θ on the shorted substrate surface. s_x is the x component of the surface slowness, and it is parallel with the crystallographic Z axis.

$LiNbO_3$, respectively. The dependence on the propagation direction of the wave is strong for both substrates. The calculated values for slowness and excitation strength agree well with those published earlier [27], [31].

The angle of the wave vector for the oblique Rayleigh-wave beams can be calculated from (12). With the pitch $p = 1.035$ μm and the frequency $f = 1781$ MHz, we obtain $s_x = 2.71 \cdot 10^{-4}$ s/m for the LSAW resonator on 42°YX-$LiTaO_3$ substrate. From the slowness curve in Fig. 5, we can determine the wave vector of the Rayleigh wave. Computing the energy flow angle, we can estimate the angle α of the Rayleigh-wave beams, emitted from the LSAW resonator (see Fig. 3), to be close to 31°.

The interferometric measurements were carried out at several frequencies to investigate the behavior of the angle of Rayleigh-wave beams. The measured and calculated radiation angles as functions of frequency are displayed in Figs. 9 and 10. While determining the experimental radiation angle at each specific frequency, information from all the beams radiated symmetrically were used. It can be seen that the numerical calculations yield angles that agree well with the experimental observations.

V. Conclusions

The amplitude profiles of the surface vibrations in the vicinity of a synchronous, one-port LSAW resonator on 42°YX-$LiTaO_3$ and in the vicinity of a synchronous, one-port longitudinal LSAW resonator on YZ-$LiNbO_3$ are studied using a scanning laser interferometer. The ampli-

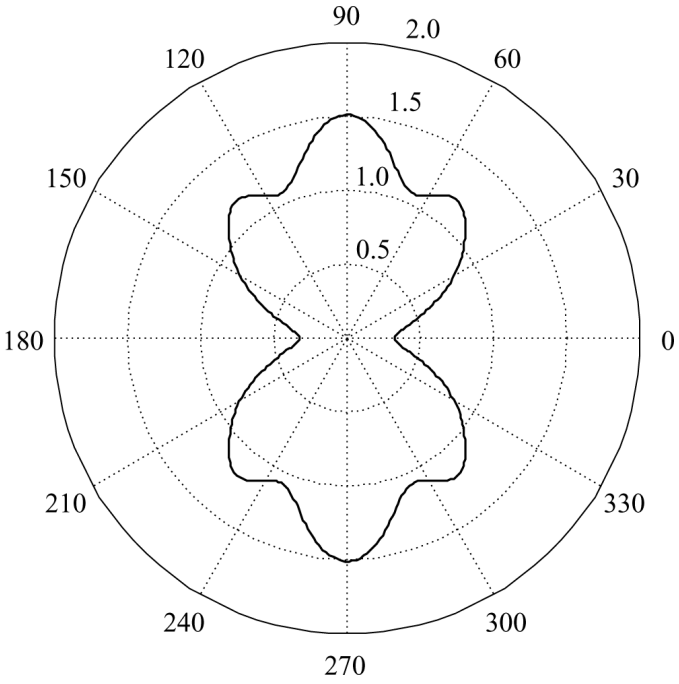

Fig. 7. Rayleigh SAW coupling strength, Γ, on the free surface of 42°Y-cut $LiTaO_3$ (in 10^6 m/F) as a function of the propagation direction θ.

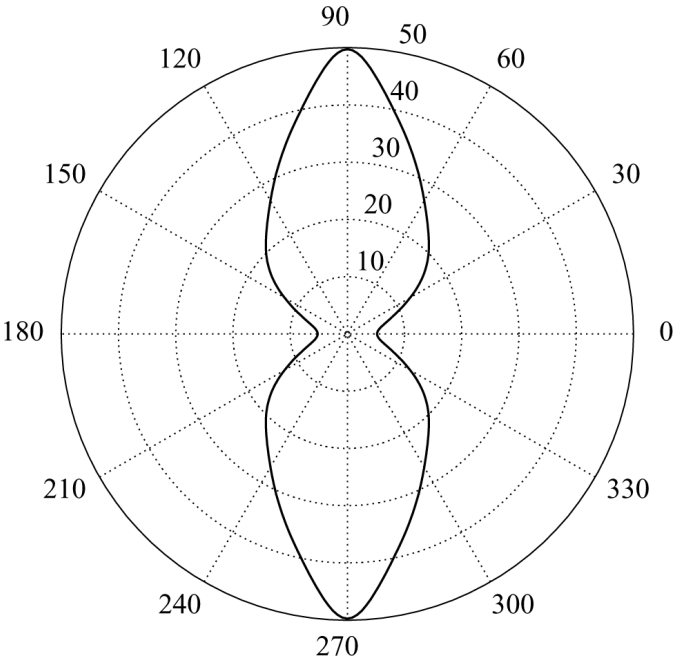

Fig. 8. Rayleigh SAW coupling strength, Γ, on the free surface of Y-cut $LiNbO_3$ (in 10^6 m/F) as a function of the propagation direction θ.

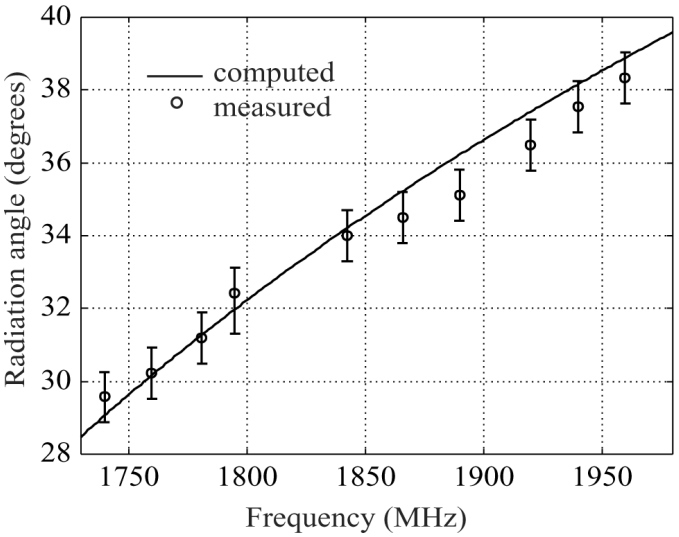

Fig. 9. Experimental and theoretical angles of radiation versus frequency for Rayleigh SAW emanating from LSAW resonator on 42°YX-$LiTaO_3$.

tude profiles reveal Rayleigh-wave beams escaping from the resonators, both in the direction perpendicular to the resonator and at oblique angles. The generation of the Rayleigh beams is attributed to the transverse electric field in the gap between the end of the electrode and the busbar, generated by the oscillating charge at the end of the electrode. A 3-D Green's-function theory is used to compute the slowness and the coupling strength of the Rayleigh SAW as a function of the propagation angle on the free surface. Based on the computed slowness curve, the angles of the Rayleigh-wave beams as a function of frequency are

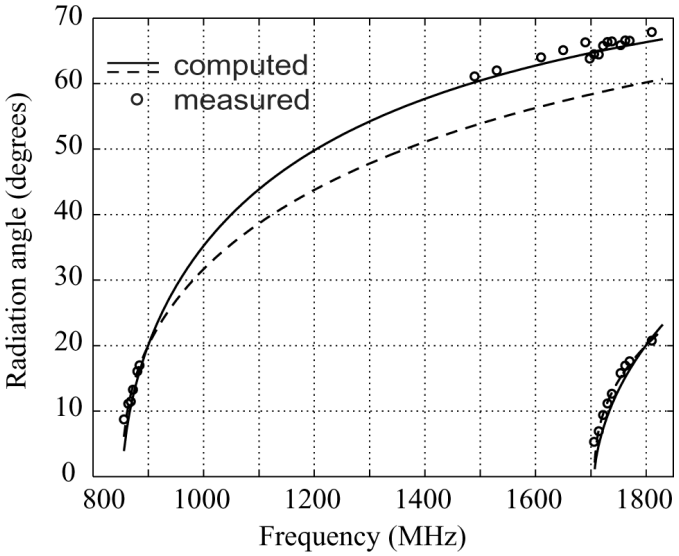

Fig. 10. Experimental and theoretical angles of radiation versus frequency for Rayleigh SAW emanating from LLSAW resonator on YZ-$LiNbO_3$. The solid line is the computed direction of the energy flow (group velocity) and dashed line is the computed direction of the wave vector (phase velocity), both for shorted surface.

predicted. The computed angles are found to agree well with those determined from the laser-probe measurements.

Using the computed coupling strength for Rayleigh waves, one can estimate the amplitude of the generated waves propagating outside the resonator. However, accurate estimates would require knowledge of the electrostatic charge distribution near the fingertips.

Usually the leakage of acoustic waves deteriorates the filter performance through increasing losses by carrying energy away from the resonator and also through acoustic crosstalk between the resonators. However, in the case of Rayleigh-wave radiation studied in this work, the effect probably is too small to cause significant losses that would deteriorate the response of the resonator. The results reveal the Rayleigh-wave radiation mechanism and provide verification through comparison between theory and experiments.

Acknowledgments

O. Holmgren thanks the Research Council of HUT and the Alfred Kordelin Foundation for scholarships. This research has been supported by the Academy of Finland. Janne Salo and Marc Solal are acknowledged for encouragement, discussions, and help. We are grateful to Julius Koskela for implementing the 2-D Green's function software used as the basis for and in the verification of the 3-D code. The authors thank their TMX colleagues for device fabrication and are grateful, in particular, to S. Chamaly for useful discussions and his interest in this work. This work has been carried out within the Eureka project E! 2442 SUMO: "New Surface Acoustic Wave Filter Generation for Mobile Telecommunications". Late Professor

Martti M. Salomaa had an important role in the research described in this article, and the authors are indebted to him for his support, encouragement, and collaboration over the years.

References

[1] O. Kawachi, S. Mineyoshi, G. Endoh, M. Ueda, O. Ikata, K. Hashimoto, and M. Yamaguchi, "Optimal cut for leaky SAW on $LiTaO_3$ for high performance resonators and filters," *IEEE Trans. Ultrason., Ferroelect., Freq. Contr.*, vol. 48, pp. 1442–1448, Sep. 2001.

[2] K. Hashimoto, M. Yamaguchi, G. Kovacs, K. C. Wagner, W. Ruile, and R. Weigel, "Effects of bulk wave radiation on IDT admittance on 42°YX-$LiTaO_3$," *IEEE Trans. Ultrason., Ferroelect., Freq. Contr.*, vol. 48, pp. 1419–1425, Sep. 2001.

[3] J. V. Knuuttila, J. Saarinen, C. S. Hartmann, V. P. Plessky, and M. M. Salomaa, "Measurement of BAW radiation from low-loss LSAW resonators," *Electron. Lett.*, vol. 37, pp. 1055–1056, Aug. 2001.

[4] J. V. Knuuttila, J. J. Vartiainen, J. Koskela, V. P. Plessky, C. S. Hartmann, and M. M. Salomaa, "Bulk-acoustic waves radiated from low-loss surface-acoustic-wave resonators," *Appl. Phys. Lett.*, vol. 84, pp. 1579–1581, Mar. 2004.

[5] J. V. Knuuttila, P. T. Tikka, C. S. Hartmann, V. P. Plessky, and M. M. Salomaa, "Anomalous asymmetric acoustic radiation in low-loss SAW filters," *Electron. Lett.*, vol. 35, pp. 1115–1116, June 1999.

[6] J. Koskela, J. V. Knuuttila, P. T. Tikka, C. S. Hartmann, V. P. Plessky, and M. M. Salomaa, "Mechanism for acoustic leakage in surface-acoustic wave resonators on rotated Y-cut lithium tantalate substrate," *Appl. Phys. Lett.*, vol. 75, pp. 2683–2685, Oct. 1999.

[7] S. Wakana, A. Miyamoto, and A. Ito, "Backside observation technique for SAW distribution under electrodes," in *Proc. IEEE Ultrason. Symp.*, 2003, pp. 1714–1717.

[8] T. Shiba, S. Oosawa, J. Hamasaki, Y. Fujita, and T. Chiba, "Low loss SAW double-mode structure suppressing spurious radiation," in *Proc. IEEE Ultrason. Symp.*, 2004, pp. 2008–2011.

[9] J. Koskela, J. V. Knuuttila, T. Makkonen, V. P. Plessky, and M. M. Salomaa, "Acoustic loss mechanisms in leaky SAW resonators on lithium tantalate," *IEEE Trans. Ultrason., Ferroelect., Freq. Contr.*, vol. 48, pp. 1517–1526, Nov. 2001.

[10] S. V. Biryukov, Y. V. Gulyaev, V. V. Krylov, and V. P. Plessky, *Surface Acoustic Waves in Inhomogeneous Media.* Berlin: Springer-Verlag, 1995, pp. 255–259.

[11] J. V. Knuuttila, J. Koskela, J. Vartiainen, and M. M. Salomaa, "BAW radiation from LSAW resonators on lithium tantalate," in *Proc. IEEE Ultrason. Symp.*, 2001, pp. 193–196.

[12] M. Kalo, "3-D Green's function theory of surface acoustic waves," Licentiate thesis, Helsinki University of Technology, Espoo, Finland, 2002.

[13] A. R. Baghai-Wadji, H. Reichinger, H. Zidek, and C. Mecklenbräuker, "Green's function applications in SAW devices," in *Proc. IEEE Ultrason. Symp.*, 1991, pp. 11–20.

[14] R. C. Peach, "A general Green function analysis for SAW devices," in *Proc. IEEE Ultrason. Symp.*, 1995, pp. 221–225.

[15] R. Peach, "On the existence of surface acoustic waves on piezoelectric substrates," *IEEE Trans. Ultrason., Ferroelect., Freq. Contr.*, vol. 48, no. 5, pp. 1308–1320, 2001.

[16] D. Qiao, W. Liu, and P. M. Smith, "General Green's functions for SAW device analysis," *IEEE Trans. Ultrason., Ferroelect., Freq. Contr.*, vol. 46, no. 5, pp. 1242–1253, 1999.

[17] P. M. Smith, "Dyadic Green's function for multi-layer SAW substrates," *IEEE Trans. Ultrason., Ferroelect., Freq. Contr.*, vol. 48, no. 1, pp. 171–179, 2001.

[18] A. Reinhardt, V. Laude, A. Khelif, and S. Ballandras, "Dyadic Green's functions of a laminar plate," *IEEE Trans. Ultrason., Ferroelect., Freq. Contr.*, vol. 51, no. 9, pp. 1157–1164, 2004.

[19] L. Wang and S. I. Rokhlin, "A compliance/stiffness matrix formulation of general Green's function and effective permittivity for piezoelectric multilayers," *IEEE Trans. Ultrason., Ferroelect., Freq. Contr.*, vol. 51, no. 4, pp. 453–463, 2004.

[20] E. L. Tan, "A robust formulation of SAW Green's functions for arbitrarily thick multilayers at high frequencies," *IEEE Trans. Ultrason., Ferroelect., Freq. Contr.*, vol. 49, no. 7, pp. 929–936, 2002.

[21] V. Laude, C. F. Jerez-Hanckes, and S. Ballandras, "Surface Green's function of a piezoelectric half-space," *IEEE Trans. Ultrason., Ferroelect., Freq. Contr.*, vol. 53, no. 2, pp. 420–428, 2006.

[22] R. F. Milsom, N. H. C. Reilly, and M. Redwood, "Analysis of generation and detection of surface and bulk acoustic waves by interdigital transducers," *IEEE Trans. Sonics Ultrason.*, vol. 24, pp. 147–166, 1977.

[23] V. I. Grigorievski, "Fast leaky surface acoustic waves on lithium niobate and lithium tantalate," in *Proc. IEEE Ultrason. Symp.*, 2000, pp. 259–262.

[24] A. Isobe, M. Hikita, and K. Asai, "Propagation characteristics of longitudinal leaky SAW in Al-grating structure," in *IEEE Trans. Ultrason., Ferroelect., Freq. Contr.*, vol. 46, pp. 849–855, July 1999.

[25] T. Makkonen, V. P. Plessky, W. Steichen, and M. M. Salomaa, "Surface-acoustic-wave devices for the 2.5–5 GHz frequency range based on longitudinal leaky waves," *Appl. Phys. Lett.*, vol. 82, pp. 3351–3353, May 2003.

[26] T. Makkonen, V. P. Plessky, W. Steichen, S. Chamaly, C. Poirel, M. Solal, and M. M. Salomaa, "Fundamental mode 5 GHz surface-acoustic-wave filters using optical lithography," *Appl. Phys. Lett.*, vol. 83, pp. 3596–3598, Oct. 2003.

[27] D. P. Morgan, *Surface-Wave Devices for Signal Processing.* Amsterdam, The Netherlands: Elsevier, 1991.

[28] J. V. Knuuttila, P. T. Tikka, and M. M. Salomaa, "Scanning Michelson interferometer for imaging surface acoustic wave fields," *Opt. Lett.*, vol. 25, pp. 613–615, May 2000.

[29] M. P. da Cunha, "Extended investigation on high velocity pseudo surface waves," *IEEE Trans. Ultrason., Ferroelect., Freq. Contr.*, vol. 45, no. 3, pp. 604–613, 1998.

[30] O. Holmgren, J. V. Knuuttila, T. Makkonen, K. Kokkonen, V. P. Plessky, W. Steichen, M. Solal, and M. M. Salomaa, "Imaging surface-acoustic fields in a longitudinal leaky wave resonator," *Appl. Phys. Lett.*, vol. 86, art. no. 024101, Jan. 2005.

[31] K. Hashimoto, *Surface Acoustic Wave Devices in Telecommunications.* Berlin: Springer-Verlag, 2000.

Olli Holmgren was born in Espoo, Finland, in 1977. He received the M.Sc. (Tech.) degree in engineering physics at the Helsinki University of Technology (TKK), Espoo, Finland, in 2003. He has worked as a research assistant and research scientist in the Materials Physics Laboratory, TKK. Currently he is working on his Dr.Sci. (Tech) thesis in the Optics and Molecular Materials Laboratory, TKK.

His research interests include laser-interferometric imaging of the vibrations in surface and bulk acoustic wave devices and in microelectromechanical systems.

Tapani Makkonen (M'98) was born in Helsinki, Finland, in 1968. He received the M.Sc., the Lic.Tech. and the Dr.Sci. (Tech.) degrees in engineering physics at the Helsinki University of Technology (TKK), Espoo, Finland, in 1996, 2001, and 2005, respectively.

From 1995 to 2005 he worked at the Materials Physics Laboratory, TKK, with modeling of SAW and BAW physics and devices. In December 2005 he joined VTI Technologies Oy, Vantaa, Finland, as a modeling specialist, working with capacitive microelectromechanical sensors. He is a corecipient of the UFFC Society 2001 Outstanding Paper Award.

Jouni V. Knuuttila was born in Marttila, Finland, in 1972. He received the M.Sc. and the Dr.Sci. (Tech.) degrees in engineering physics at the Helsinki University of Technology (TKK), Espoo, Finland, in 1998 and 2005, respectively. From 1994 to 2005 he worked at the Materials Physics Laboratory, TKK, on optical imaging of surface and bulk acoustic wave components and RF-microelectromechanical systems, sonoluminescence, and SAW prototype development.

In January 2006 he joined Nokia Multimedia Computers, Helsinki, Finland, as senior design engineer on audio and acoustics. He is a corecipient of the UFFC Society 2001 Outstanding Paper Award.

Mikko Kalo was born in Rauma, Finland, in 1973. He received the M.Sc. and the Lic.Tech. degrees in engineering physics at the Helsinki University of Technology (TKK), Espoo, Finland, in 2001 and 2002, respectively. Between 1997 and 2002 he worked at the Materials Physics Laboratory (TKK) on modeling of SAW physics and devices. Between 1997 and 2002 he also worked at the Advanced Energy Systems Laboratory (TKK) and at Teollisuuden Voima Oy, Eurajoki, Finland, on nuclear engineering. Since 2003 he has studied medicine at the University of Turku, Turku, Finland.

Victor P. Plessky (M'93–SM'01) received his Ph.D. degree in physical and mathematical sciences at the Moscow Physical-Technical Institute, Moscow, Russia, and the Dr.Sci. degree at the Institute of Radio Engineering and Electronics (IRE), Russian Academy of Sciences, Moscow, Russia, in 1978 and 1987, respectively.

Beginning in 1978, he worked at IRE, first as a junior researcher and, from 1987, as Laboratory Director. In 1991, he also worked as a part-time professor at the Patris Lumumba University, Moscow.

He received the full professor title in 1995 from the Russian Government. In 1992, he joined ASCOM Microsystems SA in Bevaix, Switzerland, where he worked as a special SAW projects manager. Since 1997, he has lectured several courses on various SAW topics at Helsinki University of Technology (TKK), Espoo, Finland, as a Visiting Professor. Currently, he holds a docentship at TKK. Since 1998 he has been working at the Neuchâtel, Switzerland, office of Thomson Microsonics (later Thales Microsonics, presently Temex) from 2002 as a consultant. He has been engaged in research on semiconductor physics, SAW physics (new types of waves, scattering and reflection on surface irregularities, laser generation of SAW), SAW device development (filters, delay lines, reflective array converters), and magnetostatic wave studies.

Dr. Plessky's current interests focus on SAW physics and low-loss SAW filter development. He is an IEEE Senior Member. He was awarded the USSR National Award for Young Scientists in 1984.

William Steichen received his engineering diploma from the "Institut National Polytechnique de Grenoble" (INPG), Grenoble, France, in 1978. He has been working for Thales Group for 22 years in the field of acoustics (underwater, medical echography, SAW and BAW devices).

He is presently working at Temex as R&D manager, SAW devices. He is a co-director of the "Laboratoire de Physique et de Microsonique," a joint laboratory between Temex and Femto-ST.